Biosensors and Bioelectronics 306 (2026) 118649

Contents lists available at ScienceDirect

Biosensors and Bioelectronics

journal homepage: www.elsevier.com/locate/bios

Surface-confined CRISPR-Cas12a biosensor with metal-enhanced fluorescence for rapid and ultrasensitive detection of SARS-CoV-2 nucleocapsid protein

Xiaoyang Han [a,1], Hong Chen [a,1], Yizeng Chang [a], Jingjing Zha [a], Ching Ying Katherine Lam [c], Mo Yang [c,d], Siu Hong Dexter Wong [a,b,*], Bohan Yin [a,b,**]

[a] School of Medicine and Pharmacy, Ocean University of China, Qingdao, 266003, China
[b] Laboratory for Marine Drugs and Bioproducts, Qingdao Marine Science and Technology Center, Qingdao, 266237, China
[c] Department of Biomedical Engineering, The Hong Kong Polytechnic University, Kowloon, Hong Kong, 999077, China
[d] Joint Research Center of Biosensing and Precision Theranostics, The Hong Kong Polytechnic University, Kowloon, Hong Kong, 999077, China

ARTICLE INFO

Keywords:
Core-shell nanoparticles
Metal-enhanced fluorescence
Localized CRISPR-Cas12a
Protein detection

ABSTRACT

CRISPR-Cas12a integrated with nanomaterials has formulated powerful biosensors for viral protein detection, addressing the urgent need for point-of-care diagnostics. However, existing platforms are hindered by either multi-step separation procedures or insufficient signal amplification, limiting their sensitivity and practicality. Here, we report a one-pot "on–off" biosensor that combines metal-enhanced fluorescence (MEF) and nanoscale spatial confinement by co-localizing both reporter substrates and the CRISPR-Cas12a system on gold–silica core–shell nanoparticles (Au@SiO_2 NPs), enabling rapid and ultrasensitive protein detection. Using SARS-CoV-2 nucleocapsid (N) protein as a model analyte, Au@SiO_2 NPs are co-functionalized with (i) ssDNA activators blocked by N protein-specific aptamers, (ii) light-up hairpin DNA (DAP) complexed with auramine O (AO) as reporters, and (iii) short polyethylene glycol (PEG) spacers to mitigate steric hindrance. The nanoplatform displays an ultrabright "on-state" fluorescence, with an intensity >860-fold higher than that of free AO, enabled by the interaction with DAP and optimized fluorophore–metal spacing (~20 nm). Upon target binding, aptamer displacement exposes the activator to locally initiate Cas12a trans-cleavage, disrupting proximal DAP structure and its interaction with AO, thereby producing a distinct "off-state" signal. Within the linear detection range, the system demonstrates up to ~85% signal reduction relative to the initial signal and a signal-to-noise ratio (SNR) of 83.89, corresponding to a ~2.5-fold higher SNR than the solution-phase system. The platform attains a limit of detection at 67.2 fg/mL within 30 min, with excellent sensitivity, selectivity, stability, and recovery in bronchoalveolar lavage fluid. By combining MEF-driven signal amplification with surface-confined CRISPR-Cas12a trans-cleavage, this platform establishes an efficient strategy for sensitive N protein detection.

1. Introduction

The global burden of infectious diseases, driven by viruses including severe acute respiratory syndrome coronavirus-2 (SARS-CoV-2), monkeypox (Mpox), and Influenza A, underscores the critical need for rapid, sensitive, and accessible diagnostics (Lamers and Haagmans, 2022; Ulaeto et al., 2023; Medina and García-Sastre, 2011). Reverse transcription polymerase chain reaction (RT-PCR) remains the gold standard for specificity, yet its reliance on complex instrumentation and trained personnel limits point-of-care applications (Yang and Rothman, 2004). Antigen detection, which targets signature viral proteins, offers a rapid and operationally feasible alternative. However, conventional formats suffer from inherent limitations: enzyme-linked immunosorbent assays, although sensitive, are labor-intensitve and cost-prohibitive (Orooji et al., 2021), whereas lateral flow assays provide rapid and equipment-free testing but lack sufficient sensitivity (Bishop et al., 2019). Thus, there is an urgent need to develop simple, rapid, and ultrasensitive biosensors for antigen detection to enhance early diagnosis.

* Corresponding author. School of Medicine and Pharmacy, Ocean University of China, Qingdao, 266003, China.
** Corresponding author. School of Medicine and Pharmacy, Ocean University of China, Qingdao, 266003, China.
E-mail addresses: dexterwong@ouc.edu.cn (S.H.D. Wong), bohanyin@ouc.edu.cn (B. Yin).
[1] Xiaoyang Han and Hong Chen contributed equally to this work.

https://doi.org/10.1016/j.bios.2026.118649
Received 17 December 2025; Received in revised form 4 March 2026; Accepted 24 March 2026
Available online 24 March 2026
0956-5663/© 2026 Elsevier B.V. All rights are reserved, including those for text and data mining, AI training, and similar technologies.

The integration of clustered regularly interspaced short palindromic repeats (CRISPR)-associated nucleases (Cas, such as Cas12a), with analytical methods has emerged as a promising strategy for biosensor development. Upon associated CRISPR RNA (crRNA)-guided recognition of its target DNA, Cas12a undergoes activation and initiates collateral and nonspecific trans-cleavage of single-stranded DNA (ssDNA) (Yin et al., 2022; Chen et al., 2024). To adapt this nucleic acid-targeting system for protein detection, diverse linkers, such as aptamers (Zhao et al., 2021; Zhang et al., 2025), aptamer-ssDNA conjugates (Li et al., 2021a,b), DNAzymes (Ding et al., 2023) and antibodies (Zhu and Zhao, 2023), have been introduced to convert protein-binding events into the exposure of ssDNA activators, enabling Cas12a-mediated trans-cleavage. Fluorescence-based readouts remain the most widely adopted detection modality due to their quantitative precision (Chen et al., 2023). For instance, Qiao et al. developed a CRISPR-Cas12a-based fluorescent biosensor that relies on competitive binding of the target toxin to an aptamer, which disrupts crRNA–aptamer duplex formation and suppresses Cas12a trans-cleavage of fluorophore–quencher ssDNA substrates, thus allowing toxin quantification (Qiao et al., 2023). Although these strategies enable protein detection, their analytical sensitivity is often limited by reliance on a single CRISPR/Cas12a-mediated amplification layer in conventional solution-phase system, without additional fluorescence enhancement or spatial organization to amplify the signal output (Song et al., 2024). Consequently, additional strategies that enhance fluorescence signal contrast and improve reaction efficiency are highly desirable.

Recent efforts have focused on optimizing CRISPR-Cas12a-based sensing performance through nanotechnology-assisted signal amplification. Nanomaterials, with their high surface-to-volume ratios, offer excellent loading capacities for DNA strands, amplifying the target protein to activator ssDNA strand ratio. Munusamy et al. developed an "on–off" fluorescent CRISPR-Cas12a biosensor using target protein-mediated assembly of antibody-modified magnetic beads and nanoparticle (NP)–dsDNA conjugates, followed by thermal release of ssDNA to activate Cas12a and generate fluorescence signal readouts (Munusamy et al., 2025). Although sensitive, the assay requires multiple incubation and separation steps and takes over 6 h to complete, increasing workflow complexity and potentially limiting point-of-care applicability. Alternatively, metallic NPs, such as gold (Au) NPs have been exploited to construct optical reporters due to their pronounced localized surface plasmon resonance (LSPR) effects. By controlling the distance between the fluorophores and metal NP surface, fluorescence can be quenched or enhanced through metal-enhanced fluorescence (MEF) (Mayer and Hafner, 2011; Hutter and Fendler, 2004). Choi et al. devised a one-step CRISPR-Cas12a nucleic acid biosensor using size-mismatched AuNPs bridged by engineered DNA linkers, enabling distance-dependent plasmonic modulation of fluorescence, including quenching and MEF (Choi et al., 2021). This dual-level amplification substantially increased the magnitude of fluorescence change relative to conventional fluorophore–quencher probes. Additionally, confining Cas12a and its ssDNA reporter substrates on NP surface further facilitates trans-cleavage (Zhang et al., 2024). Despite these advances, the synergistic combination of LSPR-mediated fluorescence modulation and spatially confined CRISPR-Cas12a system has not yet been exploited to improve protein detection performance (Table S1), representing a promising opportunity for next-generation biosensor development.

Herein, we report a rapid and ultrasensitive "on–off" biosensor that integrates CRISPR-Cas12a and MEF-based reporter positioning on Au–silica core–shell NPs (Au@SiO_2 NP) for protein detection (Fig. 1). By co-localizing activator strands, fluorescent reporters, and Cas12a machinery on the Au@SiO_2 NP surface, the platform enables dual amplification: (1) fluorescence enhancement via fluorophore–DNA interaction combined with optimized MEF, and (2) spatially confined Cas12a trans-cleavage. In contrast to biosensing strategies that rely on multi-step separation workflows or lack fluorescence signal amplification, our biosensing platform operates in a single-incubation and one-pot format, enabling direct target-triggered fluorescence attenuation with high signal contrast within 30 min.

As a model detection system, we targeted the SARS-CoV-2 nucleocapsid (N) protein using a high-affinity aptamer (Han et al., 2022). The

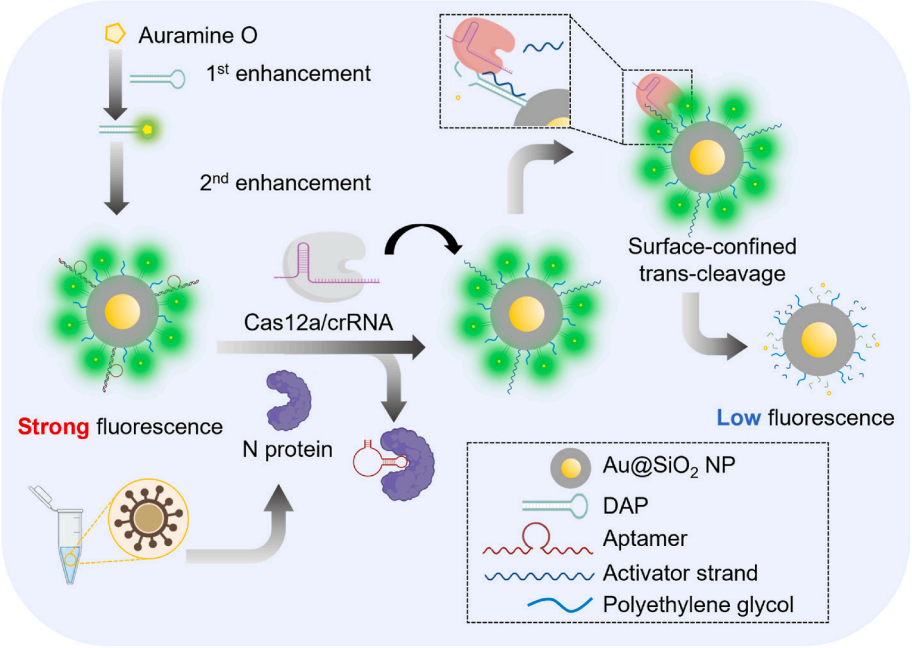


Fig. 1. Working principles of the surface-confined CRISPR-Cas12a biosensing platform with MEF-based reporter for SARS-CoV-2 N protein detection. Au@SiO_2 NPs are co-functionalized with (i) ssDNA activators blocked by N protein-specific aptamers, (ii) DAP with AO as reporter, and (iii) short PEG spacers to mitigate steric hindrance. The fluorescence signal of AO alone, remains negligible, while its interaction with DAP and further immobilization on the surface of Au@SiO_2 NPs, increase its fluorescence signal by > 860-fold, constructing an ultrabright fluorescence reporter. Upon detection, the sensing aptamer binds to the target protein due to strong affinity and exposes the surface-tethered activator, which drives localized Cas12a to trans-cleave proximal DAP loop and liberates AO into solution, resulting in a fluorescence decrease proportional to N protein concentration.

ssDNA activator is covalently immobilized on Au@SiO_2 NP surface, initially hybridized with N protein aptamer. The fluorescent reporter comprises a light-up hairpin DNA (DAP-10-42 denoted as DAP) complexed with auramine O (AO), forming a DAO complex (Kato et al., 2016). Tethering DAO complexes to the Au@SiO_2 NP (DAO–Au@SiO_2 NP) with optimized fluorophore-metal spacing induces MEF, producing a dramatic increase in fluorescence relative to free AO. While DNA immobilization introduces steric hindrance that can impede Cas12a access to the activator, the incorporation of polyethylene glycol (PEG) spacers with a molecular weight (Mw) of 350 improved the SNR, yielding a ~ 5-fold higher value than the PEG-free configuration. In the absence of N protein, DAO–Au@SiO_2 NP maintains maximal fluorescence, and aptamer–activator duplex precludes Cas12a activation. N protein dissociates the aptamer due to their stronger affinity, liberating the activator. The Cas12a/crRNA complex subsequently engages the exposed surface-tethered activator, locally trans-cleaves proximal DAP loop structure and releases AO into solution, resulting in a fluorescence decrease proportional to N protein concentration.

As summarized in Table S2, previously reported CRISPR/Cas-based protein biosensors have achieved detection limits primarily within the pg/mL–ng/mL range across electrochemical, colorimetric, and fluorescence formats. In comparison, our system achieves a limit of detection (LOD) at 67.2 fg/mL within 30 min, maintains a broad linear range (500 fg/mL–10 ng/mL), demonstrates high recovery (96–112%) in biological samples. By synergistically integrating MEF-driven fluorescence amplification with nanoscale spatial confinement of CRISPR-Cas12a system, this strategy establishes a versatile framework for rapid and ultrasensitive protein detection with potential applications in point-of-care infectious disease diagnostics.

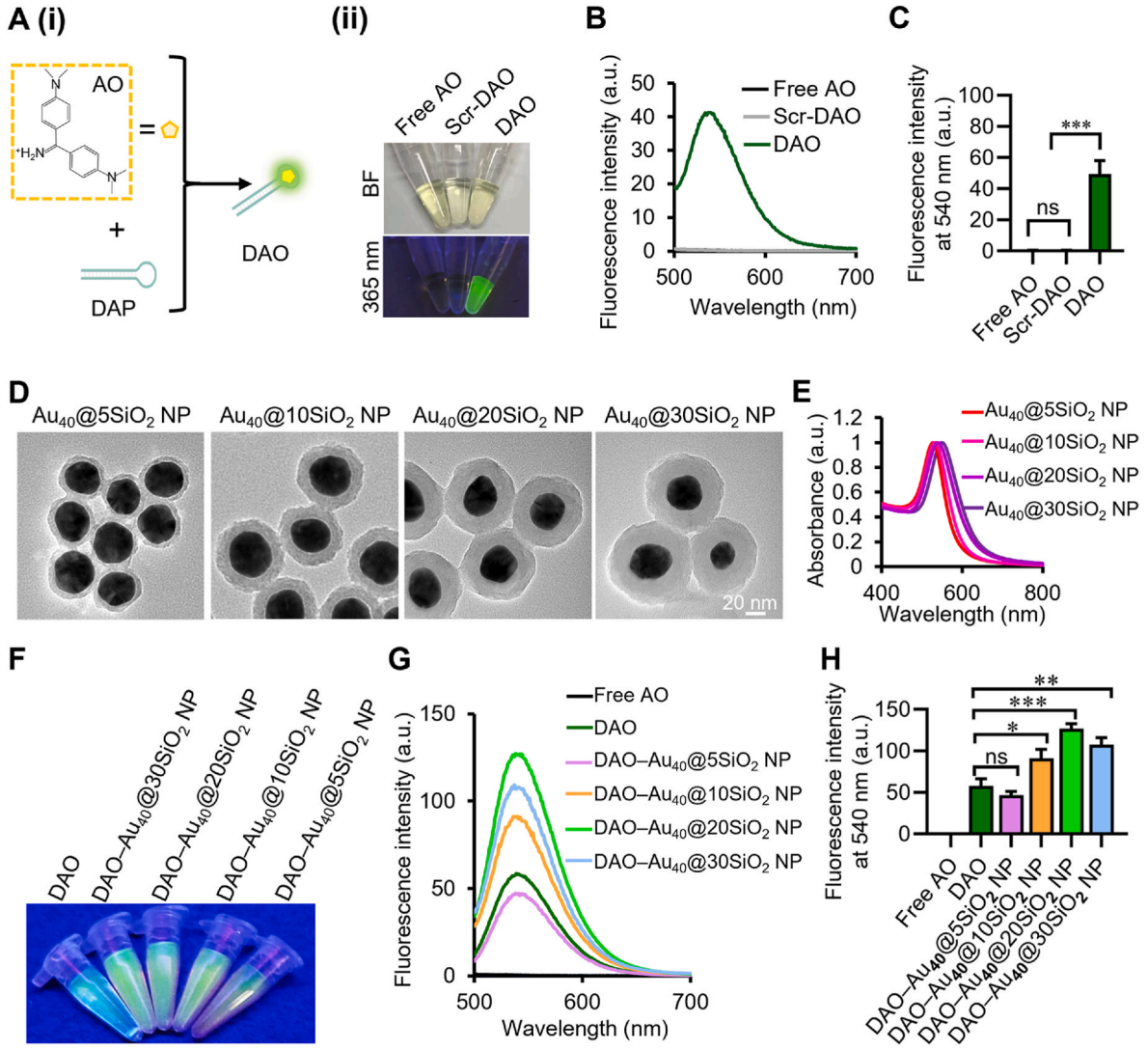


Fig. 2. Optimization of MEF-based DAO reporter in biosensing platform. (A) (i) Illustration of AO fluorescence enhancement upon interaction with DAP, and (ii) visual fluorescence of free AO, Scr-DAO and DAO under 365 nm UV illumination, confirming fluorescence enhancement of AO upon interaction with DAP. (B) Fluorescence emission spectra and (C) peak intensities at 540 nm of free AO, Scr-DAO and DAO under the 475 nm excitation (from left to right). (D) representative transmission electron microscope (TEM) images and (E) UV-visible (UV-vis) spectra of core–shell Au_{40}@$XSiO_2$ NPs (where X = 5, 10, 20, or 30 nm denotes the thickness of SiO_2 shell) modified with -NH_2 groups. The scale bar is 20 nm. (F) Representative photograph of DAO–Au_{40}@$XSiO_2$ NPs under 365 nm UV illumination. (G) Fluorescence emission spectra and (H) peak intensities at 540 nm of AO, DAO and DAO–Au_{40}@$XSiO_2$ NPs. Error bar denotes the standard deviation resulting from three independent experiments. Statistical analysis of pairwise comparison was determined by one-way ANOVA. No significance (ns): $P > 0.05$; *$P < 0.05$.; **$P < 0.01$; ***$P < 0.001$.

2. Results and discussion

2.1. Optimization of Au@SiO_2 NP for ultrabright DAO reporting via MEF

We first demonstrated that complexing AO with DAP significantly amplified AO fluorescence in aqueous solution, whereas mixing AO with a scrambled DAP sequence (Scr-DAO) produced negligible changes, as shown by fluorescence emission spectra and peak intensity at 540 nm (Fig. 2A–C). The DAO complex displayed characteristic excitation and emission maxima at 475 nm and 540 nm, respectively. Its fluorescence was readily observable under a 365 nm ultraviolet (UV) lamp, in sharp contrast to AO or Scr-DAO, which exhibited no visible signal (Fig. 2A) (Connelly et al., 2021). The fluorescence intensity scaled proportionally with DAP concentration when AO was in excess, confirming DAP as the limiting factor for signal brightness (Fig. S1).

To further amplify the DAO emission, we leveraged the LSPR effect of 40 nm AuNPs (Au_{40}NPs) (Fig. S2A and B) (Chowdhury et al., 2020). As the fluorophore–metal separation distance governs MEF efficiency, we introduced a dielectric SiO_2 spacer layer to control this gap (Zhu et al., 2018). We synthesized a series of core–shell Au_{40}@XSiO_2 NPs (where X = 5, 10, 20, or 30 nm denotes the thickness of SiO_2 shell) via a modified Stöber method, ensuring uniform and controllable shell growth (Fig. 2D and S2C). LSPR of the Au_{40}@XSiO_2 NPs exhibited progressive redshifts from 538 nm (X = 5) to 548 nm (X = 30) with increasing SiO_2 shell thickness (Fig. 2E), because the enhanced local dielectric environment altered the effective permittivity and surface electron oscillation (Gontero et al., 2017). Their surface functionalization with (3-aminopropyl)triethoxysilane exposed amine (-NH_2) groups and conferred a positive zeta potential of ~30 mV across all groups, reversing the negative charge (around −30 mV) of citrate-capped Au_{40}NPs (Fig. S3). DAO was subsequently conjugated onto the NH_2-terminated Au_{40}@XSiO_2 NPs at a fixed DAP concentration (200 strands/NP) and excess AO (DAO–Au_{40}@XSiO_2 NPs). By evaluating the fluorescence enhancement, DAO–Au_{40}@20SiO_2 NPs achieved the optimal enhancement factor (EF) of 2.32 compared to equivalent free DAO (Fig. S4), manifesting the most intense visible emission (Fig. 2F–H). In contrast, thinner shells (X = 5 nm) induced quenching (~20% signal reduction) via dominant Förster-type non-radiative energy transfer (FRET) (Yang et al., 2015), whereas thicker shells produced moderate enhancement relative to free DAO (X = 10 nm, EF = 1.58; X = 30 nm, EF = 1.68), owing to attenuated near-field coupling (Fig. 2F–H and S4). This indicates an optimal separation of ~20 nm from the Au_{40}NP core for MEF in this biosensing platform. Mere mixing DAO with Au_{40}@20SiO_2 NPs showed negligible enhancement (EF = 1.03) than free DAO (Fig. S4), confirming that precise nanoscale position of fluorophores to AuNP is critical for MEF.

To quantitatively interpret the overall signal amplification, we separated the enhancement into two experimentally resolved contributions. First, the binding of AO into the DAP hairpin produces substantial fluorescence increase. Under identical excitation and detection conditions, DAO in solution exhibits ~375-fold higher fluorescence intensity than free AO ($EF_{AO–DAP} \approx 375$). Second, distance-optimized MEF from Au_{40}@20SiO_2 NPs provides an additional enhancement factor of 2.32 relative to DAO in solution ($EF_{MEF} \approx 2.32$). The multiplicative combination of these contributions closely matches the experimentally observed overall enhancement exceeding 860-fold relative to free AO (Fig. S5), with minor deviations attributable to concentration matching and background normalization. Collectively, these results demonstrate that the ultrabright "on-state" fluorescence of DAO–Au40@20SiO_2 NPs arises from AO–DAP interaction combined with distance-optimized plasmonic amplification.

2.2. Optimization and validation of the biosensing platform for protein detection

Prior to target protein detection, all DNA sequences (Table S3) were confirmed via gel electrophoresis. Hybridization of activator strand with crRNA activates CRISPR-Cas12a, which performs trans-cleavage of the DAP loop structure, generating a cleaved residual dsDNA fragment of DAP stem structure as a lower band (Band 3) relative to intact DAP (Band 2) (Fig. 3A). Pre-hybridization of the activator with its complementary sensing aptamer formed a stable duplex (Band 1) (Fig. 3A and S6) (Zhang et al., 2023), which sequestered the activator, prevented CRISPR-Cas12a activation, and preserved intact DAP (Band 2) (Fig. 3A). We then evaluated CRISPR-Cas12a trans-cleavage performance using the DAO–Au_{40}@20SiO_2 NP reporter through fluorescence attenuation. Consistent with the gel electrophoresis results, mixing CRISPR-Cas12a/crRNA, a high concentration of activator strand (1 μM), and DAO–Au_{40}@20SiO_2 NPs resulted in a marked reduction in fluorescence emission spectrum, peak intensity at 540 nm, and visible signal under UV lamp illumination, approaching levels comparable to free AO (Fig. 3B–D). Conversely, pre-hybridized activator–aptamer duplex blocked CRISPR-Cas12a activation, and the system maintained high fluorescence similar to DAO–Au_{40}@20SiO_2 NPs alone (Fig. 3B–D), verifying the duplex stability against nonspecific CRISPR-Cas12a activation. No significant fluorescence decrease was observed during incubation at 37 °C when CRISPR-Cas12a activation was prevented by the activator–aptamer duplex, indicating that the DAO complex remains stable under the assay conditions.

To further examine whether fluorescence quenching originated from AO release, the DAO–Au_{40}@20SiO_2 NP suspension was centrifuged following CRISPR-Cas12a activation to separate the supernatant and NP pellet. Both fluorescence imaging under 365 nm illumination and emission spectra showed negligible fluorescence in the cleaved supernatant and resuspended NP pellet (Fig. S7), consistent with disruption of the DAP structure (Fig. 3A). When the collected supernatant was subsequently incubated with fresh DAP–Au_{40}@20SiO_2 NP solution, fluorescence was clearly restored. This result demonstrates that AO was present in the supernatant in its free form and regained fluorescence upon re-association with DAP, supporting AO release from DAO after Cas12a-triggered cleavage. Together, these findings indicate that CRISPR-Cas12a activation sufficiently switched the reporter from the "on" state to the "off" state through cleavage-induced disruption of the DAP loop structure and subsequent release of AO.

We next determined whether the sensing aptamer preferentially binds the N protein and dissociates from the aptamer–activator duplex to trigger CRISPR-Cas12a activation. Incubating the activator–aptamer duplex with 5 ng/mL N protein, DAO–Au_{40}@20SiO_2 NPs, and Cas12a/crRNA for 30 min resulted in a 46.7% decrease in fluorescence intensity at 540 nm compared to the N protein-absent control (W/O target group) (Fig. 3E–G). On the contrary, omission of crRNA, Cas12a, or the activator strand abolished signal changes (Fig. S8), consistent with the canonical CRISPR-Cas12a activation mechanism (Yan et al., 2025).

Subsequently, we co-immobilized the activator and DAP strands on Au_{40}@20SiO_2 NPs to construct a surface-confined system (Act/DAO–Au_{40}@20SiO_2 NPs). While the maximum DNA loading capacity was ~1500 strands per NP (Fig. S9A), a moderate loading of ~250 strands per NP at a 1:1 DAP-to-activator ratio achieved the optimal signal-to-noise ratio (SNR = 8.16), whereas further increases in DNA density reduced the SNR (Fig. S9B and C). Further optimization by varying the DAP-to-activator molar ratio on the Au_{40}@20SiO_2 NP surface showed that a 4:1 ratio displayed the optimal SNR of 17.13 upon detection (Fig. S10). Moreover, the zeta potential of Au_{40}@20SiO_2 NPs changed from positive to negative after the activator conjugation and its hybridized with the aptamer (Act–Apt/DAO–Au_{40}@20SiO_2 NPs) (Fig. S11). It is worth noting that modification of activator–aptamer duplex did not compromise the fluorescence of DAO–Au_{40}@20SiO_2 NP reporter (Fig. S12). These results suggest that excessive DNA loading may introduce steric hindrance and reduce molecular accessibility on the NP surface, thereby limiting efficient target binding and Cas12a-mediated trans-cleavage. Collectively, we verify that the SNR of our biosensing platform is optimized with its conjugated total DNA density

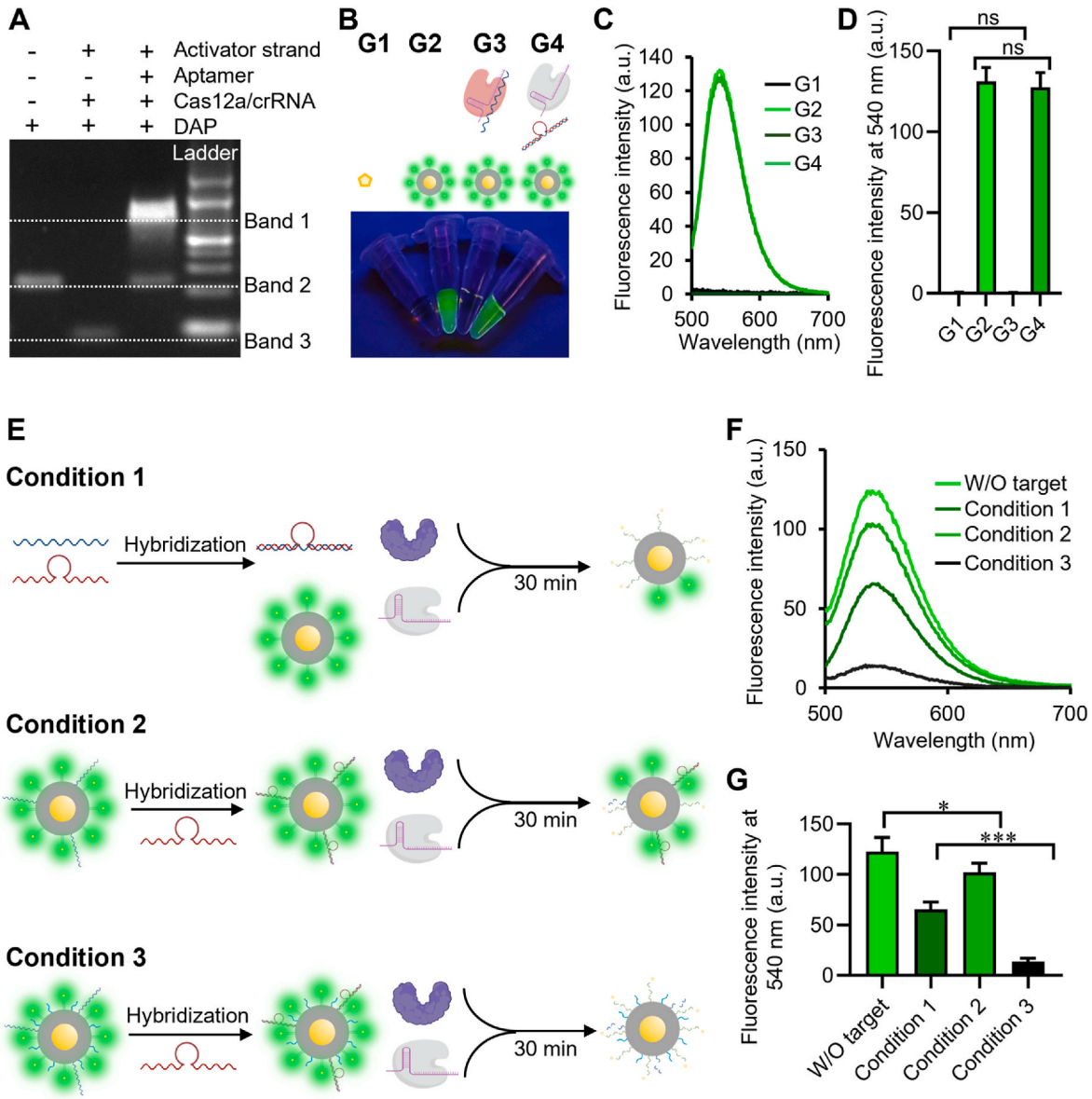


Fig. 3. Optimization of surface-confined CRISPR-Cas12a trans-cleavage activity upon target protein detection. (A) Gel electrophoresis of intact DAP (left), DAP treated with free activator and Cas12a/crRNA complex (middle), or DAP treated with activator–aptamer duplex and Cas12a/crRNA complex (right). Band 1: hybridized activator–aptamer duplex; Band 2: intact DAP; Band 3: residual dsDNA fragment of DAP. The reaction conditions were indicated in the upper panel. Trans-cleavage of CRISPR-Cas12a was validated in four experimental groups: G1 (free AO), G2 (DAO–Au_{40}@20SiO_2 NPs), G3 (DAO–Au_{40}@20SiO_2 NPs with activator and Cas12a/crRNA), and G4 (DAO–Au_{40}@20SiO_2 NPs with activator–aptamer duplex and Cas12a/crRNA). (B) Visual fluorescence under 365 nm UV illumination, (C) fluorescence emission spectra, and (D) corresponding peak intensities at 540 nm of G1–G4. (E) Comparison of CRISPR-Cas12a trans-cleavage activity and signal decrease in the presence of 5 ng/mL N protein under three conditions. Condition 1: non-confined system, free aptamer–activator duplex, DAO–Au_{40}@20SiO_2 NPs and Cas12a/crRNA complex; Condition 2: surface-confined system without PEG spacers, Act–Apt/DAO–Au_{40}@20SiO_2 NPs and Cas12a/crRNA complex; Condition 3: surface-confined system with PEG spacers, PAct–Apt/DAO–Au_{40}@20SiO_2 NPs and Cas12a/crRNA complex. (F) Fluorescence emission spectra and (G) peak intensities at 540 nm of each condition. Error bar denotes the standard deviation resulting from three independent experiments. Statistical analysis of pairwise comparison was determined by one-way ANOVA. No significance (ns): $P > 0.05$; *$P < 0.05$; ***$P < 0.001$.

and DAP-to-activator molar ratio.

2.3. PEG spacers improve surface-confined Cas12a trans-cleavage efficiency for proximal DAO disruption and enhanced signal reduction

To assess the impact of surface confinement on the performance of our biosensor, we designed two comparative groups (Fig. 3E): a non-confined system (free aptamer–activator duplexes with DAO–Au_{40}@20SiO_2 NPs) and a surface-confined system (Act–Apt/DAO–Au_{40}@20SiO_2 NPs). These two groups were separately incubated with Cas12a/crRNA and 5 ng/mL N protein. Unexpectedly, the surface-confined system presented a less pronounced fluorescence decrease and a lower SNR compared to the non-confined system (Fig. 3F,G and S13). Although the addition of 5 ng/mL N protein resulted in only ~20% decrease in fluorescence intensity, increasing the N protein concentration by 100-fold (to 500 ng/mL) did not produce a substantial additional signal reduction (Fig. S14), suggesting severe steric hindrance preventing efficient target binding and Cas12a access (Yin et al., 2022; Zhou et al., 2024).

It is well documented that the physicochemical behaviour of the PEG grafted on the material's surface depends on its molecular weight and surface density. As PEG chain length increases, the polymer occupies a

larger interfacial volume and can form thicker, more extended layers, often associated with stronger steric shielding effects. Such longer PEG chains (Mw: 2000–5000) are widely used in nanocarrier systems to reduce nonspecific adsorption and limit biomolecular access (Gomes et al., 2018; Li et al., 2021; Cruz et al., 2011; Andrian et al., 2021). In contrast, shorter PEG chains (Mw: ≤1000) generate comparatively thinner interfacial layers with weaker shielding, and are often employed as spacers to modulate nanoscale separation without substantially blocking molecular interactions (Andrian et al., 2021; Ramirez et al., 2025).

In our surface-confined system, the interactions among Act–Apt/DAO constructs may induce local steric hindrance, restricting efficient target binding and Cas12a access. Therefore, our design objective was not only to create a strong shielding layer, but rather to introduce moderate spatial separation to alleviate hindrance while preserving molecular accessibility. Based on this rationale, PEG (Mw: 350) was selected, as its estimated contour length (<2.5 nm) is comparable to the DAP stem length (~2.62 nm), allowing controlled spacing without shielding the DAP loop sequence (Lostao et al., 2023; Ambia-Garrido et al., 2010). Additionally, a poly-thymine spacer (~15.75 nm) was introduced between the activator strand and the NP surface to further improve exposure of the aptamer and activator domains (Table S3).

To experimentally validate this design, we functionalized Act–Apt/DAO–Au_{40}@20SiO_2 NPs with a gradient of PEG densities (0, 200, 400, 600, and 800 strands per NP) and evaluated their detection efficacy against 500 ng/mL N protein (Fig. S15A). This PEG modification (PAct–Apt/DAO–Au_{40}@20SiO_2 NPs) did not alter zeta potential and baseline fluorescence (Figs. S11 and S12). Strikingly, PEG incorporation dose-dependently enhanced aptamer–protein binding and Cas12a trans-cleavage, leading to progressive fluorescence decreases upon detection of N protein (Fig. S15B). At 800 PEGs/NP, the post-detection signal of the sensing platform dropped to levels comparable to free AO (Fig. S15C). This optimal PEG-spaced platform (SNR = 83.89) exhibited fluorescence decreases 86% and 383% greater than those of the non-confined (SNR = 33.41) and PEG-free confined systems (SNR = 16.76), respectively, corresponding to ~ 2.5-fold and 5.0-fold higher SNRs (Fig. 3E–G and S13). These results demonstrate that PEG spacers effectively alleviate steric constraints and enhance performance of the surface-confined biosensing platform.

2.4. Sensitivity and selectivity study of the biosensing platform

We first optimized PAct–Apt/DAO–Au_{40}@20SiO_2 NPs concentration for detection, identifying that 0.5 nM achieved maximal SNR (Fig. S16). The sensitivity of the biosensor was then assessed across a broad concentration range of N protein (50 fg/mL–500 ng/mL). Significant signal decrease was observed at concentrations as low as 100 fg/mL, with saturation above 100 ng/mL within 30 min (Fig. 4A–C and S17) (Ding et al., 2020). Quantitative analysis revealed a linear correlation between the blank-corrected fluorescence changes and the logarithm of N protein

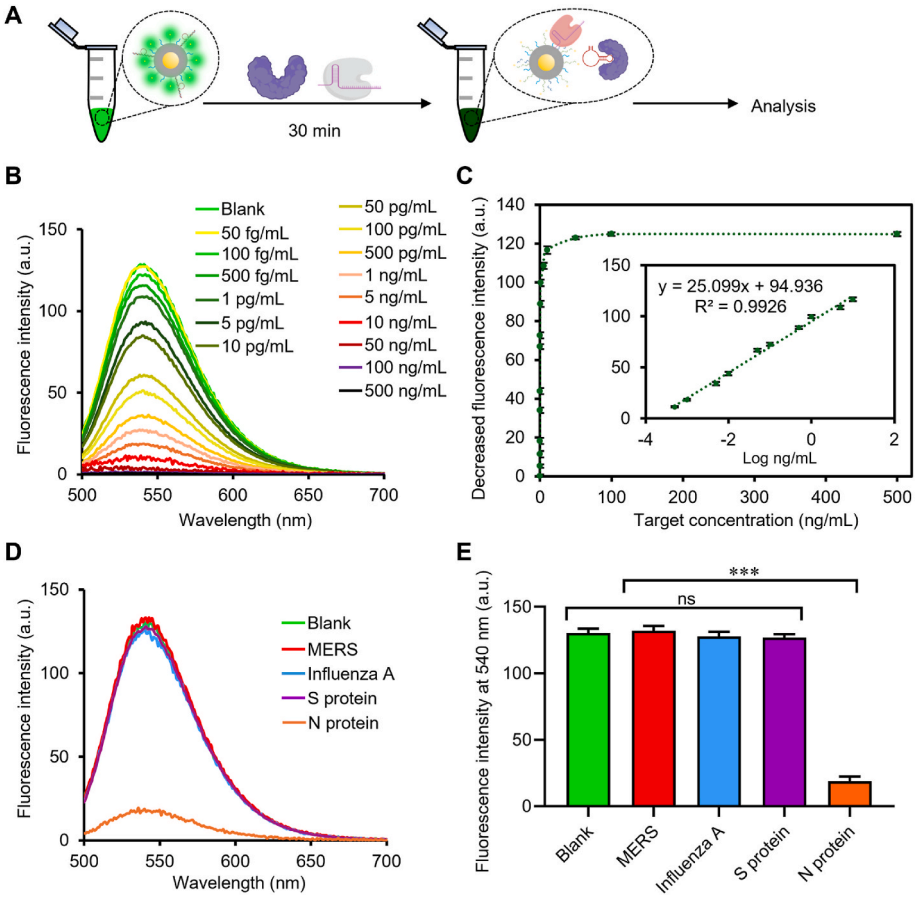


Fig. 4. Sensitivity study of detecting N protein using the surface-confined biosensing platform with PEG spacers. (A) Illustration of one-pot detection procedure using the biosensing platform within 30 min. (B) Fluorescence emission spectra of the biosensing platform after detection of blank samples (N protein-free control) and N protein at varying concentrations (50 fg/mL–500 ng/mL), displayed from top to bottom. (C) Plot of the decreased intensities at 540 nm versus the log concentration of N protein, corresponding to (B). The inset shows the corresponding linear calibration curve (500 fg/mL–10 ng/mL). (D) Fluorescence emission spectra and (E) peak intensities at 540 nm of the biosensing platform after detection of blank sample, 100 ng/mL nontarget viral proteins (MERS, influenza A, and SARS-CoV-2 S protein), and 5 ng/mL N protein. Error bar denotes the standard deviation resulting from three independent experiments. Statistical analysis of pairwise comparison was determined by one-way ANOVA. No significance (ns): $P > 0.05$; ***$P < 0.001$.

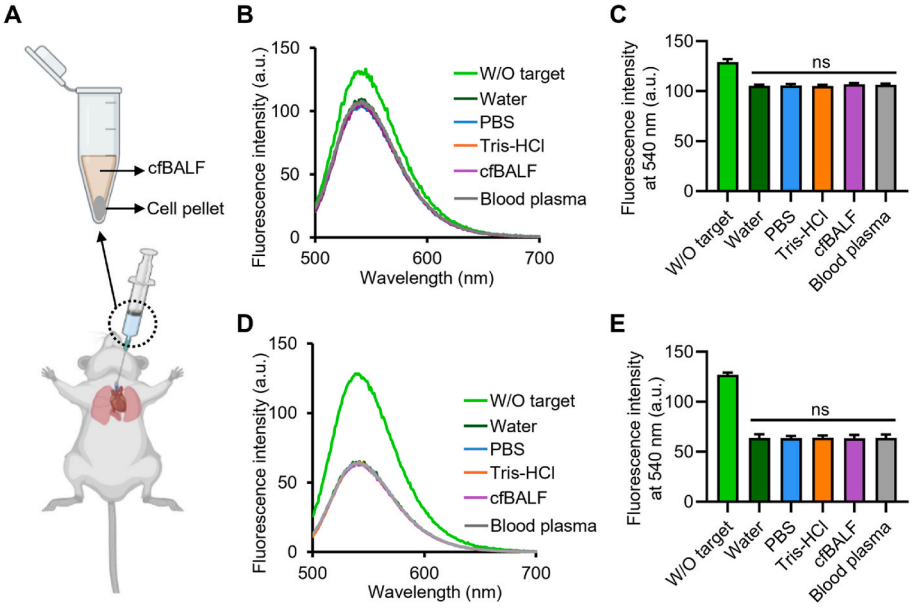
concentrations from 500 fg/mL to 10 ng/mL ($R^2 = 0.9926$) (Fig. 4C and S17). The calculated LOD was 67.2 fg/mL (3σ/m criterion), with excellent reproducibility as evidenced by low relative standard deviation (%RSD) values (Fig. S18). In contrast, a non-confined system failed to reliably distinguish 500 fg/mL from background noise (Fig. S19), highlighting the essential role of nanoscale confinement and PEG spacing in concentrating reactants for ultrasensitive detection (Luo et al., 2022; Wang et al., 2023).

We further examined the detection selectivity of the biosensing platform by challenging with nontarget viral proteins (MERS, influenza A, and SARS-CoV-2 spike protein at 100 ng/mL) (Fig. 4D and E). The result revealed that only the target N protein (5 ng/mL) induced a substantial (~85%) fluorescence reduction relative to the initial signal, and signals for non-targets were statistically indistinguishable from the blank control (Fig. 4D and E). This high specificity is attributed to the precise recognition of sensing aptamer, which selectively disrupts the inhibitory aptamer–activator complex only in the presence of the target protein, thereby triggering CRISPR-Cas12a-mediated trans-cleavage of the DAO reporter.

2.5. Stability and performance of the biosensing platform in complex biological matrices

We systematically evaluated the long-term storage stability of our biosensor at 4 °C in the dark over 28 days. Over the first 14 days, fluorescence intensity remained highly stable with less than 10% reduction (Fig. S20A–C), indicating minimal degradation or detachment of surface-immobilized DNA. Importantly, when stored biosensing platforms were subjected to 5 ng/mL N protein and Cas12a/crRNA complex, the target-induced fluorescence decreasing response was preserved over 28 days of storage, with post-detection signal similar to those of fresh samples (Figs. S20A,D,E). These data confirm that storage (within 14 days) does not compromise reporter integrity, aptamer–target binding, CRISPR-Cas12a activation and trans-cleavage efficiency.

Finally, we studied the performance of our biosensing platform in clinically relevant matrices or standard buffers, including murine blood plasma, cell-free bronchoalveolar lavage fluid (cfBALF), phosphate-buffered saline (PBS) and Tris-HCl buffer (Yin et al., 2019).



F

Condition	Expected concentration	Measured concentration	Recovery (%)	RSD% (n=3)
PBS (pH 7.4)	1 pg/mL	1.069 pg/mL	106.88	7.15
	50 pg/mL	53.97 pg/mL	107.95	1.05
Tris-HCl buffer (pH 7.4)	1 pg/mL	1.111 pg/mL	111.13	9.07
	50 pg/mL	51.63 pg/mL	103.27	0.94
cfBALF	1 pg/mL	0.965 pg/mL	96.47	8.32
	50 pg/mL	55.87 pg/mL	111.77	1.64
Blood plasma	1 pg/mL	0.995 pg/mL	99.46	9.63
	50 pg/mL	54.39 pg/mL	108.77	1.59

Fig. 5. Detection of N protein in complex biological matrices using the biosensing platform. (A) Illustration of cfBALF collected from naïve Balb/c mice. (B) Fluorescence emission spectra and (C) peak intensities at 540 nm of the biosensing platform after incubation with either protein-free sample (W/O target) or 1 pg/mL N protein spiked into cfBALF, blood plasma, PBS and Tris-HCl buffer. (D) Fluorescence emission spectra and (E) peak intensities at 540 nm after challenging with either protein-free sample or 50 pg/mL N protein in the same four matrices. (F) Anti-interference performance of the biosensing platform for detecting N protein under various conditions. Error bar denotes the standard deviation resulting from three independent experiments. Statistical analysis of pairwise comparison was determined by one-way ANOVA. No significance (ns): $P > 0.05$.

Remarkably, the platform reliably detected N protein at 1 pg/mL and 50 pg/mL across all matrices, with no significant matrix-dependent variation in signal response (Fig. 5A–E). Blank controls (matrices alone) displayed consistently strong "on-state" fluorescence, indistinguishable from W/O target group (Fig. S21), indicating minimal non-specific interference. In addition, spike-and-recovery experiments demonstrated excellent reproducibility, with recovery rates of 96–112% and %RSD values below 10% across all matrices (Fig. 5F). This stability ensures reliable signal readouts even in the presence of abundant non-target proteins and complex lipid biomolecules. Together, these results justify our MEF-based CRISPR-Cas12a biosensing platform as a rapid, ultrasensitive, highly specific, matrix-tolerant, and reproducible approach with excellent stability for direct N protein detection in biological fluids.

3. Conclusion

We developed a spatially engineered CRISPR-Cas12a biosensing platform that converts N protein detection from a conventional solution-phase reaction into a surface-confined nanoscale process. By co-localizing the CRISPR-Cas12a machinery and a bright reporter (DAO) within a precisely tuned MEF field on $Au_{40}@SiO_2$ NPs, the platform integrates plasmonic fluorescence amplification with localized trans-cleavage in a single, one-pot system. The DAO complex provides an ultrabright "on-state" signal through the interaction between AO and light-up DNA, while optimized fluorophore–metal spacing enhances baseline emission. Upon target recognition, activator exposure initiates Cas12a cleavage in close proximity to the reporter, disrupting DAP structure and releasing AO to generate a distinct "off-state" signal. This combination of fluorescence amplification and spatially confined CRISPR-Cas12a trans-cleavage produces a pronounced signal contrast compared to conventional solution-phase CRISPR-Cas12a system. Beyond analytical performance, this work highlights the potential of nanoscale spatial organization to couple fluorescence amplification with localized CRISPR activation for high-contrast signal transduction. Although demonstrated here using SARS-CoV-2 N protein as a model target and relying on aptamer-based recognition, the proposed design strategy provides a modular framework that can be potentially adapted for rapid and ultrasensitive protein detection with appropriate optimization.

CRediT authorship contribution statement

Xiaoyang Han: Data curation, Formal analysis, Writing – original draft. **Hong Chen:** Data curation, Formal analysis, Writing – original draft. **Yizeng Chang:** Methodology. **Jingjing Zha:** Validation. **Ching Ying Katherine Lam:** Methodology. **Mo Yang:** Funding acquisition, Supervision. **Siu Hong Dexter Wong:** Conceptualization, Funding acquisition, Supervision, Writing – review & editing. **Bohan Yin:** Conceptualization, Funding acquisition, Supervision, Writing – review & editing.

Declaration of competing interest

The authors declare that they have no known competing financial interests or personal relationships that could have appeared to influence the work reported in this paper.

Acknowledgements

We would like to acknowledge the funding from National Natural Science Foundation of China (32501158), Start-up Fundings of Ocean University of China (862401013154 and 862401013155), Laboratory for Marine Drugs and Bioproducts Qingdao Marine Science and Technology Center (no.: LMDBCXRC202401 and LMDBCXRC202402), Taishan Scholar Youth Expert Program of Shandong Province (tsqn202306102 and tsqn202312105), Shandong Provincial Overseas Excellent Young Scholar Program (2024HWYQ-042 and 2024HWYQ-043), Shenzhen Science and Technology Program-Basic Research Scheme (JCYJ20220531090808020), the Hong Kong Research Grants Council (RGC) Collaborative Research Fund (C5005-23W and C5078-21E), the RGC Hong Kong General Research Fund (15217621 and 15216622), the Hong Kong Polytechnic University Internal Fund (CEB1, WZ5Z, YWDU, W02C, CDKU, WZB6, W43P and WZDH) for supporting this work.

Appendix A. Supplementary data

Supplementary data to this article can be found online at https://doi.org/10.1016/j.bios.2026.118649.

Data availability

Data will be made available on request.

References

Ambia-Garrido, J., Vainrub, A., Pettitt, B.M., 2010. A model for structure and thermodynamics of ssDNA and dsDNA near a surface: a coarse grained approach. Comput. Phys. Commun. 181 (12), 2001–2007.
Andrian, T., Pujals, S., Albertazzi, L., 2021. Quantifying the effect of PEG architecture on nanoparticle ligand availability using DNA-PAINT. Nanoscale Adv. 3 (24), 6876–6881.
Bishop, J.D., Hsieh, H.V., Gasperino, D.J., Weigl, B.H., 2019. Sensitivity enhancement in lateral flow assays: a systems perspective. Lab Chip 19 (15), 2486–2499.
Chen, H., Tan, Y., Feng, Y., Liu, F., Tan, C., Xu, N., Jiang, Y., Tan, Y., 2024. Universal smartphone-assisted label-free CRISPR/Cas12a-DNAzyme chemiluminescence biosensing platform for on-site detection of nucleic acid and non-nucleic acid targets. Biosens. Bioelectron. 247, 115929.
Chen, H., Zhuang, Z., Chen, Y., Qiu, C., Qin, Y., Tan, C., Tan, Y., Jiang, Y., 2023. A universal platform for one-pot detection of circulating non-coding RNA combining CRISPR-Cas12a and branched rolling circle amplification. Anal. Chim. Acta 1246, 340896.
Choi, J.-H., Lim, J., Shin, M., Paek, S.-H., Choi, J.-W., 2021. CRISPR-Cas12a-based nucleic acid amplification-free DNA biosensor via Au nanoparticle-assisted metal-enhanced fluorescence and colorimetric analysis. Nano Lett. 21 (1), 693–699.
Chowdhury, A.D., Nasrin, F., Gangopadhyay, R., Ganganboina, A.B., Takemura, K., Kozaki, I., Honda, H., Hara, T., Abe, F., Park, S., Suzuki, T., Park, E.Y., 2020. Controlling distance, size and concentration of nanoconjugates for optimized LSPR based biosensors. Biosens. Bioelectron. 170, 112657.
Connelly, R.P., Madalozzo, P.F., Mordeson, J.E., Pratt, A.D., Gerasimova, Y.V., 2021. Promiscuous dye binding by a light-up aptamer: application for label-free multi-wavelength biosensing. Chem. Commun. 57 (30), 3672–3675.
Cruz, L.J., Tacken, P.J., Fokkink, R., Figdor, C.G., 2011. The influence of PEG chain length and targeting moiety on antibody-mediated delivery of nanoparticle vaccines to human dendritic cells. Biomaterials 32 (28), 6791–6803.
Ding, L., Wu, Y., Liu, L.-e., He, L., Yu, S., Effah, C.Y., Liu, X., Qu, L., Wu, Y., 2023. Universal DNAzyme walkers-triggered CRISPR-Cas12a/Cas13a bioassay for the synchronous detection of two exosomal proteins and its application in intelligent diagnosis of cancer. Biosens. Bioelectron. 219, 114827.
Ding, X., Yin, K., Li, Z., Lalla, R.V., Ballesteros, E., Sfeir, M.M., Liu, C., 2020. Ultrasensitive and visual detection of SARS-CoV-2 using all-in-one dual CRISPR-Cas12a assay. Nat. Commun. 11, 4711.
Gomes, C.P., Leiro, V., Lopes, C.D.F., Spencer, A.P., Pêgo, A.P., 2018. Fine tuning neuronal targeting of nanoparticles by adjusting the ligand grafting density and combining PEG spacers of different length. Acta Biomater. 78, 247–259.
Gontero, D., Veglia, A.V., Bracamonte, A.G., Boudreau, D., 2017. Synthesis of ultraluminescent gold core–shell nanoparticles as nanoimaging platforms for biosensing applications based on metal-enhanced fluorescence. RSC Adv. 7 (17), 10252–10258.
Han, C., Li, W., Li, Q., Xing, W., Luo, H., Ji, H., Fang, X., Luo, Z., Zhang, L., 2022. CRISPR/Cas12a-Derived electrochemical aptasensor for ultrasensitive detection of COVID-19 nucleocapsid protein. Biosens. Bioelectron. 200, 113922.
Hutter, E., Fendler, J.H., 2004. Exploitation of localized surface plasmon resonance. Adv. Mater. 16 (19), 1685–1706.
Kato, T., Shimada, I., Kimura, R., Hyuga, M., 2016. Light-up fluorophore–DNA aptamer pair for label-free turn-on aptamer sensors. Chem. Commun. 52 (21), 4041–4044.
Lamers, M.M., Haagmans, B.L., 2022. SARS-CoV-2 pathogenesis. Nat. Rev. Microbiol. 20, 270–284.
Li, H., Li, M., Yang, Y., Wang, F., Wang, F., Li, C., 2021. Aptamer-linked CRISPR/Cas12a-based immunoassay. Anal. Chem. 93 (6), 3209–3216.
Li, M., Jiang, S., Simon, J., Paßblick, D., Frey, M.-L., Wagner, M., Mailänder, V., Crespy, D., Landfester, K., 2021. Brush conformation of polyethylene glycol determines the stealth effect of nanocarriers in the low protein adsorption regime. Nano Lett. 21 (4), 1591–1598.

Lostao, A., Lim, K., Pallarés, M.C., Ptak, A., Marcuello, C., 2023. Recent advances in sensing the inter-biomolecular interactions at the nanoscale – a comprehensive review of AFM-based force spectroscopy. Int. J. Biol. Macromol. 238, 124089.
Luo, T., Li, J., He, Y., Liu, H., Deng, Z., Long, X., Wan, Q., Ding, J., Gong, Z., Yang, Y., Zhong, S., 2022. Designing a CRISPR/Cas12a- and au-nanobeacon-based diagnostic biosensor enabling direct, rapid, and sensitive miRNA detection. Anal. Chem. 94 (17), 6566–6573.
Mayer, K.M., Hafner, J.H., 2011. Localized surface plasmon resonance sensors. Chem. Rev. 111 (6), 3828–3857.
Medina, R.A., García-Sastre, A., 2011. Influenza A viruses: new research developments. Nat. Rev. Microbiol. 9, 590–603.
Munusamy, S., Zheng, H., Jahani, R., Zhou, S., Chen, J., Kong, J., Guan, X., 2025. DNA-assisted CRISPR-Cas12a enhanced fluorescent assay for protein detection in complicated matrices. ACS Appl. Bio Mater. 8 (1), 754–762.
Orooji, Y., Sohrabi, H., Hemmat, N., Oroojalian, F., Baradaran, B., Mokhtarzadeh, A., Mohaghegh, M., Karimi-Maleh, H., 2021. An overview on SARS-CoV-2 (COVID-19) and other human coronaviruses and their detection capability via amplification assay, chemical sensing, biosensing, immunosensing, and clinical assays. Nano-Micro Lett. 13, 18.
Qiao, Y., Wang, X., Song, Y., Zhang, J., Han, Q., 2023. CRISPR-Cas12a-based aptasensor for sensitive and selective FB1 detection. J. Food Compos. Anal. 123, 105615.
Ramirez, M.A., Bou-Gharios, J., Freis, B., Draussin, J., Cheignon, C., Charbonnière, L.J., Laurent, S., Gevart, T., Gasser, A., Jung, S., Rossetti, F., Tillement, O., Noel, G., Pivot, X., Detappe, A., Bégin-Colin, S., Harlepp, S., 2025. Spacer engineering in nanoparticle–peptide conjugates boosts targeting specificity for tumor-associated antigens. Nanoscale 17 (9), 5021–5032.
Song, Y.-L., He, X.-L., Pan, M.-M., Wang, M., Jiang, M., Xu, L., Yu, X., 2024. An ultrasensitive biosensor with suppressed background signals for FEN1 detection in a homogeneous reaction via Cascade primer exchange reaction and CRISPR/Cas12a system. Sens. Actuators, B 403, 135194.
Ulaeto, D., Agafonov, A., Burchfield, J., Carter, L., Happi, C., Jakob, R., Krpelanova, E., Kuppalli, K., Lefkowitz, E.J., Mauldin, M.R., Oliveira, T., Onoja, B., Otieno, J., Rambaut, A., Subissi, L., Yinka-Ogunleye, A., Lewis, R.F., 2023. New nomenclature for mpox (monkeypox) and monkeypox virus clades. Lancet Infect. Dis. 23 (3), 273–275.
Wang, X., Mu, X., Li, J., Liu, G., Zhao, S., Tian, J., 2023. A novel nanoparticle surface-constrained CRISPR-Cas12a 3D DNA walker-like nanomachines for sensitive and stable miRNAs detection. Anal. Chim. Acta 1251, 340950.
Yan, J., Yin, B., Zhang, Q., Li, C., Chen, J., Huang, Y., Hao, J., Yi, C., Zhang, Y., Wong, S. H.D., Yang, M., 2025. A CRISPR-Cas12a-mediated dual-mode luminescence and colorimetric nucleic acid biosensing platform based on upconversion nanozyme. Biosens. Bioelectron. 270, 116963.
Yang, Y., Huang, J., Yang, X., Quan, K., Wang, H., Ying, L., Xie, N., Ou, M., Wang, K., 2015. FRET nanoflares for intracellular mRNA detection: avoiding false positive signals and minimizing effects of system fluctuations. J. Am. Chem. Soc. 137 (26), 8340–8343.
Yang, S., Rothman, R.E., 2004. PCR-based diagnostics for infectious diseases: uses, limitations, and future applications in acute-care settings. Lancet Infect. Dis. 4 (6), 337–348.
Yin, B., Chan, C.K.W., Liu, S., Hong, H., Wong, S.H.D., Lee, L.K.C., Ho, L.W.C., Zhang, L., Leung, K.C.-F., Choi, P.C.-L., Bian, L., Tian, X.Y., Chan, M.N., Choi, C.H.J., 2019. Intrapulmonary cellular-level distribution of inhaled nanoparticles with defined functional groups and its correlations with protein corona and inflammatory response. ACS Nano 13 (12), 14048–14069.
Yin, B., Zhang, Q., Xia, X., Li, C., Ho, W.K.H., Yan, J., Huang, Y., Wu, H., Wang, P., Yi, C., Hao, J., Wang, J., Chen, H., Wong, S.H.D., Yang, M., 2022. A CRISPR-Cas12a integrated SERS nanoplatform with chimeric DNA/RNA hairpin guide for ultrasensitive nucleic acid detection. Theranostics 12 (13), 5914–5930.
Zhang, L., Luo, S., Li, W., Su, W., Chen, S., Liu, C., Pan, W., Situ, B., Zheng, L., Li, L., Yan, X., Zhang, Y., 2024. Co-freezing localized CRISPR-Cas12a system enables rapid and sensitive nucleic acid analysis. J. Nanobiotechnol. 22, 602.
Zhang, Q., Yin, B., Hao, J., Ma, L., Huang, Y., Shao, X., Li, C., Chu, Z., Yi, C., Wong, S.H. D., Yang, M., 2023. An AIEgen/graphene oxide nanocomposite (AIEgen@GO)-based two-stage "turn-on" nucleic acid biosensor for rapid detection of SARS-CoV-2 viral sequence. Aggregate 4 (1), e195.
Zhang, T., Zhao, Y., Zhu, C., Zhu, X., Zhu, X., Qiu, Y., Nie, Z., Lei, C., 2025. CRISPR/Cas12a protein switch powered label-free electrochemical biosensor for sensitive viral protease detection. Anal. Chem. 97 (14), 8039–8047.
Zhao, X., Li, S., Liu, G., Wang, Z., Yang, Z., Zhang, Q., Liang, M., Liu, J., Li, Z., Tong, Y., Zhu, G., Wang, X., Jiang, L., Wang, W., Tan, G.-Y., Zhang, L., 2021. A versatile biosensing platform coupling CRISPR–Cas12a and aptamers for detection of diverse analytes. Sci. Bull. 66 (1), 69–77.
Zhou, S., Ran, J., Man, S., Zhang, J., Yuan, R., Yang, X., 2024. Exploring the effect of steric hindrance on trans-cleavage activity of CRISPR-cas12a for ultrasensitive SERS detection of P53 DNA. Anal. Chem. 96 (26), 10654–10661.
Zhu, J., Chang, H., Li, J.-J., Li, X., Zhao, J.-W., 2018. Using silicon-coated gold nanoparticles to enhance the fluorescence of CdTe quantum dot and improve the sensing ability of mercury (II). Spectrochim. Acta, Part A 188, 170–178.
Zhu, F., Zhao, Q., 2023. CRISPR/Cas12a-powered competitive immunosorbent assay for small molecules. Anal. Chem. 95 (39), 14720–14726.